Exp. Anim. 66(3), 271–282, 2017

—Original—

A novel missense mutation of *Mip* causes semi-dominant cataracts in the *Nat* mouse

Gou TAKAHASHI[1)], Sayaka HASEGAWA[1)], Yukiko FUKUTOMI[2)], Chihiro HARADA[2)], Masamune FURUGORI[1)], Yuta SEKI[3)], Yoshiaki KIKKAWA[3)], and Kenta WADA[1–3)]

[1)]*Graduate School of Bioindustry, Tokyo University of Agriculture, 196 Yasaka, Abashiri, Hokkaido 099-2493, Japan*
[2)]*Department of Bioproduction, Tokyo University of Agriculture, 196 Yasaka, Abashiri, Hokkaido 099-2493, Japan*
[3)]*Mammalian Genetics Project, Department of Genome Medicine, Tokyo Metropolitan Institute of Medical Science, 2-1-6 Kamikitazawa, Setagaya-ku, Tokyo 156-8506, Japan*

Abstract: Major intrinsic protein of lens fiber (MIP) is one of the proteins essential for maintaining lens transparency while also contributing to dominant cataracts in humans. The Nodai cataract (*Nat*) mice harbor a spontaneous mutation in *Mip* and develop early-onset nuclear cataracts. The *Nat* mutation is a c.631G>A mutation (Mip^{Nat}), resulting in a glycine-to-arginine substitution (p.Gly211Arg) in the sixth transmembrane domain. The $Mip^{Nat/Nat}$ homozygotes exhibit congenital cataracts caused by the degeneration of lens fiber cells. MIP normally localizes to the lens fiber cell membranes. However, the $Mip^{Nat/Nat}$ mice were found to lack an organelle-free zone, and the MIP was mislocalized to the nuclear membrane and perinuclear region. Furthermore, the $Mip^{Nat/+}$ mice exhibited milder cataracts than $Mip^{Nat/Nat}$ mice due to the slight degeneration of the lens fiber cells. Although there were no differences in the localization of MIP to the membranes of lens fiber cells in $Mip^{Nat/+}$ mice compared to that in wild-type mice, the protein levels of MIP were significantly reduced in the eyes. These findings suggest that cataractogenesis in Mip^{Nat} mutants are caused by defects in MIP expression. Overall, the Mip^{Nat} mice offer a novel model to better understand the phenotypes and mechanisms for the development of cataracts in patients that carry missense mutations in MIP.
Key words: congenital cataract, MIP, missense mutation, mouse, semi-dominant cataract

Introduction

The major intrinsic protein of lens fiber (MIP), also known as Aquaporin 0 (AQP0), is a member of the aquaporin family which is composed of at least 12 related proteins [33]. The aquaporin family of proteins has six transmembrane α-helices, forms homo-tetramers in the cell membranes, and plays a role in water channel activity in the cell plasma membrane in multiple organs [4, 28]. MIP is known as the lens-specific aquaporin protein [4, 8, 21], and is one of the most abundant proteins in the lens, which constitutes up to 60% of the membrane proteins found in the lens. MIP also acts to maintain transparency in the lens by playing a role in water channel activity and cell-cell gap junctions [4, 20].

Mutations in human *MIP* are known to be responsible for human dominant cataracts, and many types of mutations in *MIP* have been reported [3, 4, 7, 8, 10, 13, 16, 19, 20, 25, 26, 30, 36, 37, 40–43]. Berry *et al.* first reported two missense mutations (p.Glu134Gly and p. Thr138Arg) in *MIP* that caused human congenital cataracts. These mutations were in the fourth transmembrane region of the MIP protein, each resulting in different pathologies [3, 8]. The $MIP^{p.Thr138Arg}$ mutation resulted

(Received 24 January 2017 / Accepted 27 March 2017 / Published online in J-STAGE 24 April 2017)
Address corresponding: K. Wada, Faculty of Bioindustry, Tokyo University of Agriculture, 196 Yasaka, Abashiri, Hokkaido, 099-2493, Japan
Supplementary Table: refer to J-STAGE: https://www.jstage.jst.go.jp/browse/expanim

in a progressive, bilateral, punctate lens opacity that was limited to the mid- and peripheral lamellae [8]. The *MIP*$^{p.Glu134Gly}$ mutation resulted in a fine, non-progressive congenital lamellar and structural opacification [8]. In addition, Gu *et al.* reported that a *MIP*$^{p.Arg33Cys}$ mutation resulted in total cataracts, which is characterized by bilateral, complete opacification of the fetal nucleus and cortex [13]. Other reports have also shown that mutations in *MIP* exhibited polymorphic phenotypes, such as punctate and nuclear cataracts [18, 35]. Therefore, different mutations in *MIP* can lead to varying degrees of lens opacity [3], and missense mutations in *MIP* account for over half of the mutations reported in patients with cataracts [17].

In mice, four mutant alleles of *Mip* (*Mip*$^{Cat\text{-}Fr}$ [27], *Mip*$^{Cat\text{-}Lop}$ [27], *Mip*^{Hfi} [29], and *Mip*$^{Cat\text{-}Tohm}$ [23]) have been reported to develop semi-dominant cataracts. These mouse models are important resources in understanding the detailed pathology of human cataracts that are caused by mutations in *MIP*. The *Mip*$^{Cat\text{-}Lop}$ and *Mip*$^{Cat\text{-}Fr}$ alleles were the first reported mouse mutant alleles of *Mip*. The *Mip*$^{Cat\text{-}Lop}$ allele contains a missense mutation (c.151G>C) which results in an alanine-to-proline (p. Ala51Pro) substitution [27]. The *Mip*$^{Cat\text{-}Fr}$ allele results in a transposon-induced splicing error that substitutes a long terminal repeat (LTR) sequence for the carboxyl-terminus of MIP [27]. The *Mip*^{Hfi} and *Mip*$^{Cat\text{-}Tohm}$ alleles contain in-frame mutations that result in the deletion of 55 and 4 amino acids in MIP, respectively [23, 29]. The *Mip*$^{Cat\text{-}Fr}$ allele was predicted to be a loss-of-function allele, whereas the *Mip*$^{Cat\text{-}Lop}$, *Mip*^{Hfi} and *Mip*$^{Cat\text{-}Tohm}$, alleles result in dominant-negative effects [23, 27–29]. In addition to these spontaneous mutations, a *Mip* null mutant (*Mip*$^{-/-}$) mice have also been produced [28]. Overall, MIP haploinsufficiency leads to dominant cataract formation.

Recently, we isolated the Nodai cataract (*Nat*) mouse, a spontaneous mutant exhibiting lens opacity, from our SJL/J mouse strain colony. Here, we report that a novel missense mutation in *Mip* is responsible for congenital cataracts in *Nat* mice, resulting in abnormal MIP expression in the perinuclear region of the lens fiber cells. The profound lens opacity and lens fiber degeneration were confirmed in the lens of *Nat*/*Nat* homozygotes at an early age, indicating that the mutant phenotype for *Nat* homozygous mice is similar to that of previously reported *Mip* mutant mice. In contrast, *Nat*/+ heterozygotes mice had mild lens fiber degeneration without grossly diagnosable lens opacity. The lens phenotypes in *Nat*/+ mice were also notably milder than that of other *Mip* mutants. Thus, the *Nat* mice constitute a potential novel model for studying the pathological features of patients with cataracts caused by missense mutations in *Mip*.

Materials and Methods

Ethics statement

All of the procedures involving animals met the guidelines described in the Proper Conduct of Animal Experiments, as defined by the Science Council of Japan, and were approved by the Animal Care and Use Committee on the Ethics of the Tokyo University of Agriculture (Approval number: 270048).

Mouse husbandry

We used wild-type SJL/J mice (Charles River Laboratories Japan, Yokohama, Japan) in all experiments. The *Nat* mutant was first identified in a litter in the SJL/J colony. The founder mutant mouse was crossed to a SJL/J mouse, and the F_2 offspring with severe lens opacity were isolated and maintained by sibling matings at the Tokyo University of Agriculture. For all of the phenotypic and expression analyses, we used *Nat*/+ mouse that were generated by mating wild-type and *Nat* mice on the SJL/J background. For the genetic analysis, the *Nat*/*Nat* mice were crossed to the BALB/cAJcl (BALB/cA) strain (CLEA Japan, Tokyo, Japan) to generate backcross progeny.

Gross diagnosis of the lens phenotype

The pupillary dilatation was conducted using Mydrin-P (Santen Pharmaceutical, Osaka, Japan), and both eyes were observed after 5 min. After euthanasia, the eyeballs were excised, and the presence or absence of lens opacity was diagnosed by observations under dark-field microscopy using the Leica M60 stereomicroscope (Leica Microsystems, Wetzlar, Germany).

Histological analysis and immunohistochemistry

The eyeballs were excised from the mice after being euthanized by cervical dislocation and were fixed by Superfix (Kurabo, Osaka, Japan), dehydrated in methanol, embedded in paraffin, and sectioned (5 μm) as previously described [34, 35, 38]. After removing the paraffin, the sections were stained with haematoxylin and

eosin, and then were observed using a Leica DM2500 light microscope (Leica Microsystems). The eyeball paraffin sections were also used for immunohistochemistry as previously described [34, 35, 38]. The primary antibodies for AQP0 (1:300, Alpha Diagnostic International, catalog #AQP01-S-A-P) and CTNNB1 (1:500, BD Biosciences, catalog #610154) used in this study were obtained commercially and had been characterized in previous studies [38]. The fluorescent images were obtained using a Leica TCS SP5 confocal laser-scanning microscope (Leica Microsystems), Zeiss LSM780 confocal microscope (Carl Zeiss, Jena, Germany), and BZ-X700 fluorescence microscope (Keyence, Osaka, Japan).

Linkage analysis and mutation analysis

To identify the *Nat* locus by linkage analysis, we generated backcross progeny by mating between SJL/J-*Nat*/*Nat* mice with (BALBc/A x SJL/J-*Nat*/*Nat*) F_1 mice. Genomic DNA was extracted from the livers and was genotyped by multiple microsatellite markers located throughout the mouse genome. PCR were performed with the KAPA2G Fast PCR Kit (Kapa Biosystems, Woburn, MA, USA) according to the manufacturer's protocol. The PCR products were separated on a 4% agarose (3% Agarose KANTO HC, Kanto Chemical, Tokyo, Japan and 1% Agarose S, Nippon gene, Tokyo, Japan) gel as previously described [38].

The *Nat* mutation in *Mip* was confirmed by DNA sequencing of the PCR products. Four coding exons of *Mip* were amplified in wild-type, *Nat*/+, and *Nat*/*Nat* mice by AmpliTaq Gold DNA polymerase (Thermo Fisher Scientific, Waltham, MA, USA) with the primer sets as shown in Table S1. PCR products were purified using the QIAquick Gel Extraction Kit (Qiagen, Valencia, CA, USA), and were sequenced using a 3730 × l DNA analyzer (Thermo Fisher Scientific).

For genotyping the *Nat* allele, we performed PCR restriction fragment length polymorphisms (PCR-RFLP) analysis by using genomic DNAs from the *Nat* mutants, SJL/J, C57BL/6J, C3H/HeN, DBA/2J, NOD/Shi, BALB/cA, and KOR/Stm mice. Exon 4 of *Mip* was amplified via PCR with the following primer pair: exon4RFLP_F and exon4RFLP_R (Table S1). The resulting 575-bp DNA fragment was digested by the restriction enzyme *Bsl*I (New England Biolabs, Ipswich, MA, USA). The PCR products were then separated on a 4% agarose gel [38].

Bioinformatics analysis

Alignments of the MIP were performed using Clustal X [18]. The effect of the *Nat* mutation was assessed using by S-VAR (http://p4d-info.nig.ac.jp/s-var/), which is provided the automatic tools, SIFT [22], PolyPhen-2 [1] and PROVEAN [6], for predicting the possible impact of the amino acid substitutions.

An electron crystallographic structure of MIP (PBD: 2B6O) [11] was utilized as a template to model the *Nat* mutation. The ribbon and B-spline diagrams were created using SWISS-MODEL (http://swissmodel.expasy.org/) and Waals software (Altif Labs, Inc., Tokyo, Japan).

Quantitative RT-PCR

Total RNAs from postnatal day 0 (P0) eyes were extracted by using the RNeasy mini kit (Qiagen), and approximately 2 μg of total RNA treated by DNase I (Takara Bio, Kusatsu, Japan) was used for cDNA synthesis with the Superscript VILO cDNA synthesis kit (Thermo Fisher Scientific). The quantitative RT-PCR was performed using QuantiTect Primer Assays (Qiagen) and the 7500 Fast Real-Time PCR System (Thermo Fisher Scientific). Biological replicates of the RNA samples were obtained from three individuals. The signal values were normalized to the *Gapdh* signals, and the geometric means of the target signals were calculated in triplicate. The wild-type expression level was assigned an arbitrary value of 1. The results were presented as the mean ± standard deviation (SD). Statistical analysis was performed by one-way ANOVA with Turkey's HSD test using R (https://www.r-project.org/) (**P<0.01).

Immunoblotting

The insoluble protein fraction from P1 eyes of wild-type, *Nat*/+, and *Nat*/*Nat* mice were extracted as previously described [37]. Approximately 2.5 μg of protein was separated on a 10% SDS-polyacrylamide gel, and then transferred to a PVDF membrane (GE Healthcare Japan, Tokyo, Japan). The MIP protein bands were detected using the anti-AQP0 antibody (1:1,000), followed by a HRP-anti-rabbit IgG secondary antibody (1:20,000). ECL Prime Western blotting detection regents (GE Healthcare Japan) were used for the enhanced chemiluminescent detection of the specifically bound antibody. CTNNB1 was used as an internal control, and was detected using the CTNNB1 (1:500) antibody and HRP-anti-mouse IgG secondary antibody (1:20,000). Three biological replicates of MIP were analyzed using western

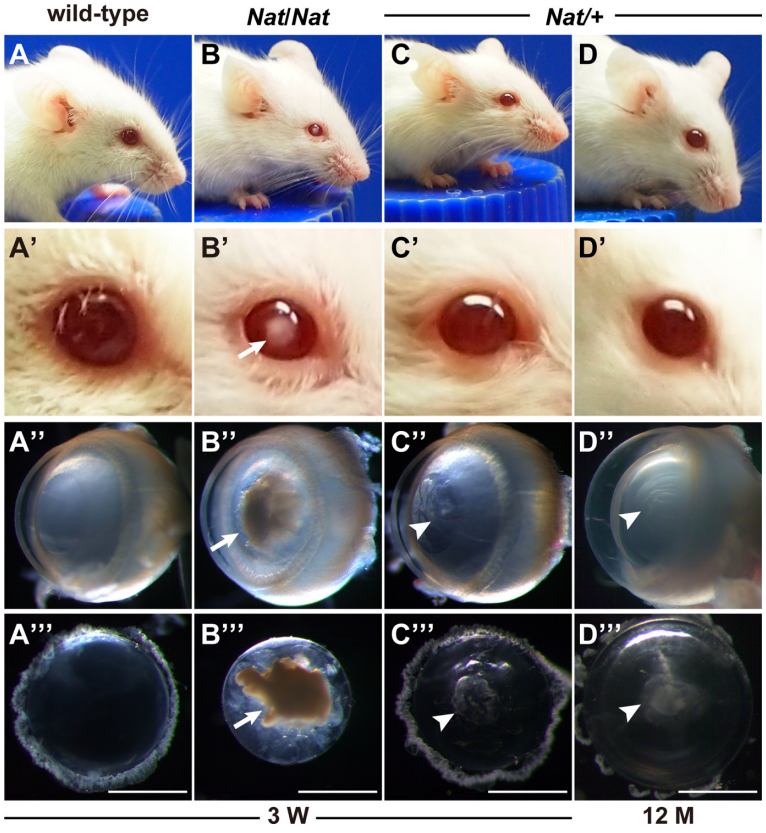

Fig. 1. Lens opacities in *Nat* mutant mice. A–D. Gross appearances of the eyes among the wild-type (A), *Nat*/*Nat* homozygous (B) and *Nat*/+ heterozygous (C and D) mice at 3 weeks (A–C) and 12 months (D) of age. The magnified images in the area of eyes are shown in A'–D'. A''–D'''. Phenotypic comparisons via dark field microscopy of the diagonal side views of the eyes (A''–C'') and the anterior views of the lens among each mouse at 3 weeks of age (A'''–C''') and *Nat*/+ heterozygous mouse at 12 months of age (D'' and D'''). Arrows and arrowheads indicate profound lens opacities in *Nat*/*Nat* mice and mild disorganization of the lens fibers in *Nat*/+ mice, respectively. Scale bar=1 mm.

blot and quantified via ImageJ (http://rsb.info.nih.gov/ij). The wild-type expression level was assigned an arbitrary value of 1. The results were presented as the mean ± SD, and statistical analysis was performed by Welch's *t* test (***P*<0.01).

Results

Cataract phenotypes of Nat mutant mice

All *Nat*/*Nat* homozygous mice exhibited severe lens opacity within one month after birth. The normal lens transparency found in wild-type mice is shown in Fig. 1A and 1A'. In contrast, the lens opacities in *Nat*/*Nat* homozygous mice are shown in Fig. 1B and B'. A comparison of the extirpated eyes and lenses between the wild-type and *Nat*/*Nat* mice confirmed the severe lens opacity in *Nat*/*Nat* mice (Figs. 1A'', 1A''', 1B'' and 1B'''). Moreover, a remarkable size reduction in the *Nat*/*Nat* lens was observed (Fig. 1B'''). Meanwhile, *Nat*/+ heterozygous mice did not exhibit lens opacity by gross diagnosis until at least 12 months after birth (Figs. 1C, 1C', 1D and 1D'). However, a slight degeneration and lens opacity were detected at 3 weeks and 12 months of age in *Nat*/+ heterozygous mouse under dark-field microscopy (Figs. 1C'', 1C''', 1D'' and 1D''').

To investigate the histological defects in the lens of *Nat* mutants, we analyzed paraffin-embedded sections of the eye in the wild-type, *Nat*/*Nat*, and *Nat*/+ mice. At P0, the normal development of the lens fibers was observed in wild-type mice (Fig. 2A). In contrast, the *Nat*/*Nat* mice already displayed mild degeneration and swollen cells in the lens fiber at P0 (Fig. 2B). Although the normally aligned lens fiber cells were observed in wild-type mice at P30 (Fig. 2D), in comparison, *Nat*/*Nat* mice

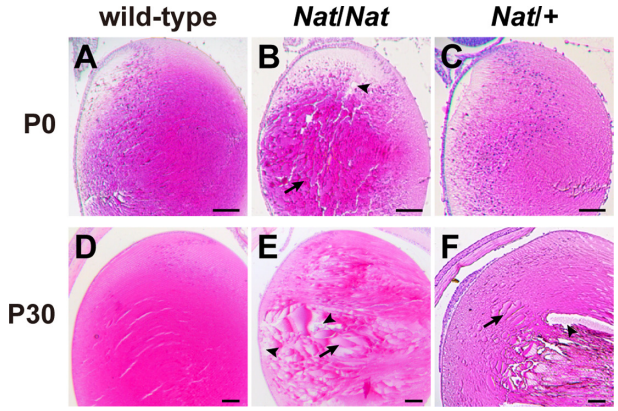

Fig. 2. Lens histology in *Nat* mutant mice. A comparison of the histological lens phenotypes among the wild-type (A and D), *Nat*/*Nat* (B and E), and *Nat*/+ mice (C and F) at P0 (A–C) and P30 (D–F). Arrows and arrowheads indicate the swelling of the lens fiber cells and small vacuoles on the lens fibers, respectively. Scale bar=100 μm.

had severe degeneration, large swollen cells, and small vacuoles (Fig. 2E). Furthermore, in *Nat*/+ mice, normal lens fibers were observed at P0 (Fig. 2C). By P30, we detected a degeneration of the lens in all of the tested *Nat*/+ mice (n=3), but the phenotypes were milder than that of the *Nat*/*Nat* mice (Fig. 2F).

Identification of the Nat mutation

To identify the causative mutation for cataractogenesis in *Nat* mice, we produced 56 (BALB × SJL/J-*Nat*/*Nat*) F_1 × SJL/J-*Nat*/*Nat* backcross progeny and diagnosed the lens phenotypes at P30. The affected and unaffected individuals were segregated in a 1:1 ratio (26:30, P>0.5). We performed linkage mapping with 58 microsatellite markers throughout the mouse chromosomes 1–19 on 19 backcross progeny mice. The analysis revealed a linkage association with the region between the telomere and 118.2 Mb on chromosome 10 (Fig. 3A). Although this genomic interval contains more than 190 protein coding genes (Ensembl: GRCm38.p5), we hypothesized that there was a mutation in *Mip* in the *Nat* mutants because mutation in *Mip* have been shown to be responsible for cataracts in humans [3, 4, 7, 8, 10, 13, 16, 19, 20, 25, 26, 30, 36, 37, 40–43], mice [23, 27–29], and rat [38]. We analyzed all the exon sequences of *Mip* that were amplified from genomic DNA of wild-type, *Nat*/+, and *Nat*/*Nat* mice, and identified a 1-bp substitution at nucleotide position 631 in exon 4 of *Mip*(c.631G>A) in the *Nat* mutants (Fig. 3B). Moreover, PCR-RFLP analysis using *Bsl*I showed a homozygous c.631G genotype of *Mip* in all of the tested inbred strains. An undigested fragment representing the mutant allele was only observed in mice carrying the *Nat* mutation. In addition, we genotyped the (BALB × SJL/J-*Nat*/*Nat*) F_1 × SJL/J-*Nat*/*Nat* backcross progeny using by PCR-RFLP analysis to ensure that the phenotypes of the progeny correlated with their genotypes. The results indicate that unaffected and affected phenotypes of 56 backcross progeny completely correlated with their heterozygous and homozygous genotypes, respectively (Fig. 3A and data not shown). The c.631G>A mutation is a missense mutation that results in a glycine-to-arginine substitution at position 211 (p.Gly211Arg) in the sixth transmembrane (*H6*) domain of MIP (Figs. 3B and 3D). Fig. 3D also shows the site and types of mutations identified in humans, mice, and rat. The $MIP^{p.Asp213Valfs*46}$ [10], $MIP^{p.Gly215Asp}$ [7], and $MIP^{p.Tyr219*}$ [30] mutant alleles have also been found in the *H6* domain in humans, and the $Mip^{p.Val203fs*60}$ ($Mip^{Cat\text{-}Fr}$) allele was identified in mice [27]. These mutations are frameshift mutations except for the $MIP^{p.Gly215Asp}$ allele; therefore, the *Nat* allele is the first reported case of a missense mutation affecting the *H6* domain of the MIP protein in mice.

The Gly211 residue is highly conserved across species from fish to mammals, as shown by an alignment of MIP orthologs (Fig. 4A). Moreover, the p.Gly211Arg mutation was predicted to damage the *H6* domain of MIP as analyzed by the SIFT (score=0), PolyPhen2 (score=1.0), and PROVEAN (score=−6.89) algorithms. Therefore, we constructed a mutant model using a high-resolution crystal structure of MIP (PBD: 2B6O) [11] (Fig. 4B) to predict the structural effects of the p.Gly211Arg mutation in *Nat* mice. The p.Gly211Arg mutation converts a neutral residue to a positively charged residue (Fig. 4B), suggesting that the p.Gly211Arg mutation may affect neighboring conformations of the MIP structure. We simulated the conformational changes by structural modeling. The analysis indicated that there is a probability for the Arg211 residue to charge and crash into the Glu134 residue and *H4* domain because of the space constraints (Fig 4C and 4D). These results strongly suggested that *Nat* mice develop cataracts because of the p.Gly211Arg mutation in *Mip* and thus is a novel mutant allele of *Mip*.

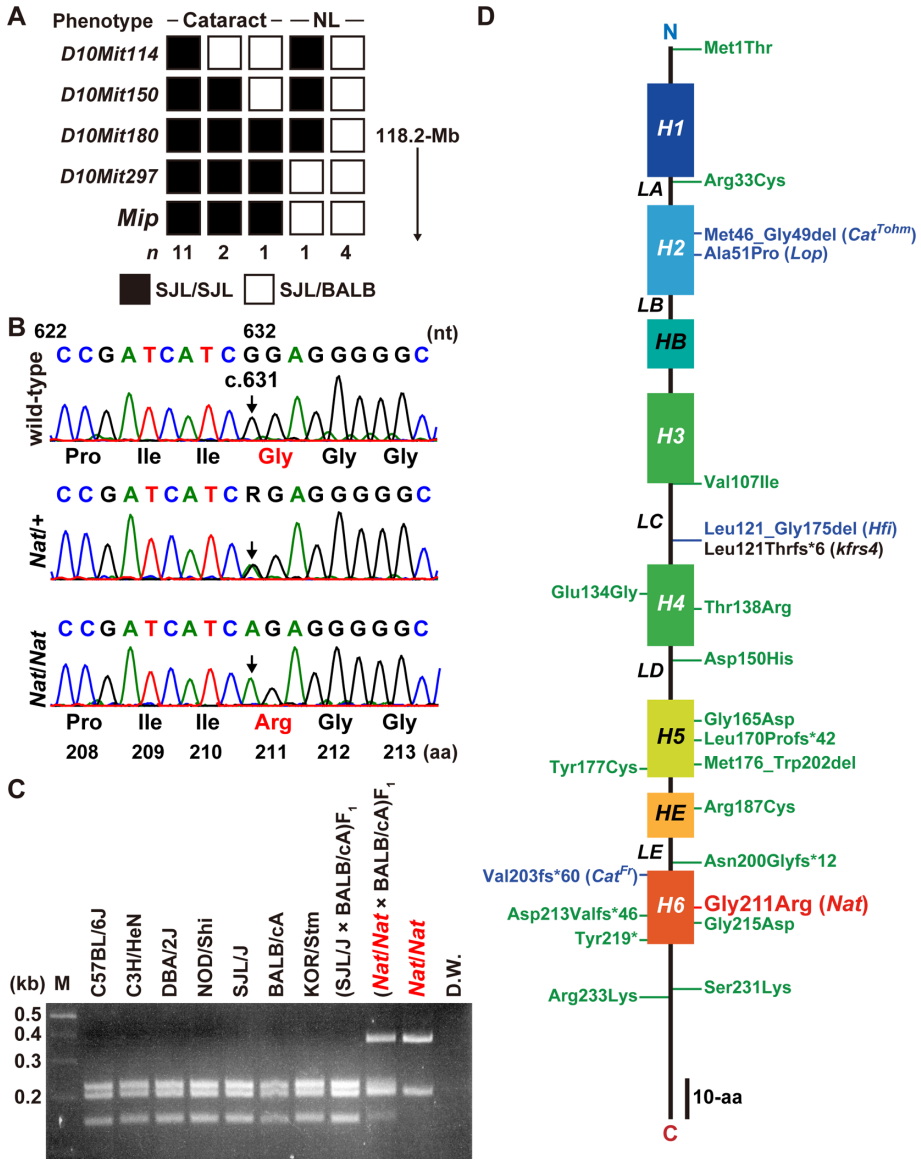

Fig. 3. The *Nat* mutation in *Mip*. A. Mapping of the *Nat* locus. The diagram shows the fine-mapping results for the genomic interval between the telomere and 118.2 Mb region on chromosome 10 that was linked to the normal and cataract phenotypes observed in [(SJL/J-*Nat*/*Nat* × BALB/cA) F_1 × SJL/J-*Nat*/*Nat*] backcrossed mice. NL: normal lens. B. Sequence analysis of the wild-type, *Nat*/+, and *Nat*/*Nat* mice revealing a c.631G>A substitution (arrows) in *Mip*, resulting in a p.Gly211Arg substitution. C. The c.631G>A introduces a *Bsl*I site, facilitating genotyping of the mice via PCR-RFLP analysis. M: size standard (100-bp ladder). D. Schematic diagram of the MIP secondary structure showing the locations of the mutations in humans (green), mice (blue), and rat (black). The six transmembrane domains (*H1*, *H2*, *H3*, *H4*, *H5,* and *H6*), two hemichannels (*HB* and *HE*), and the extracellular (*LA*, *LC,* and *LE*) and intracellular (*LB* and *LD*) loops are indicated.

Effects of the Mip^{Nat} allele on Mip transcript and protein expression

To estimate the effect of the c.631G>A mutation on *Mip* transcription, we relatively quantified *Mip* mRNA in the eyes of wild-type, $Mip^{Nat/+}$ heterozygous, and $Mip^{Nat/Nat}$ homozygous mice. Although there were no differences in the expression levels between the wild-type and $Mip^{Nat/+}$ mice, *Mip* transcript levels in $Mip^{Nat/Nat}$ mice were significantly decreased compared with those of wild-type and $Mip^{Nat/+}$ mice (Fig. 5A). Next, we performed western blot analysis to investigate the effects of the p.Gly211Arg mutation on MIP protein expression

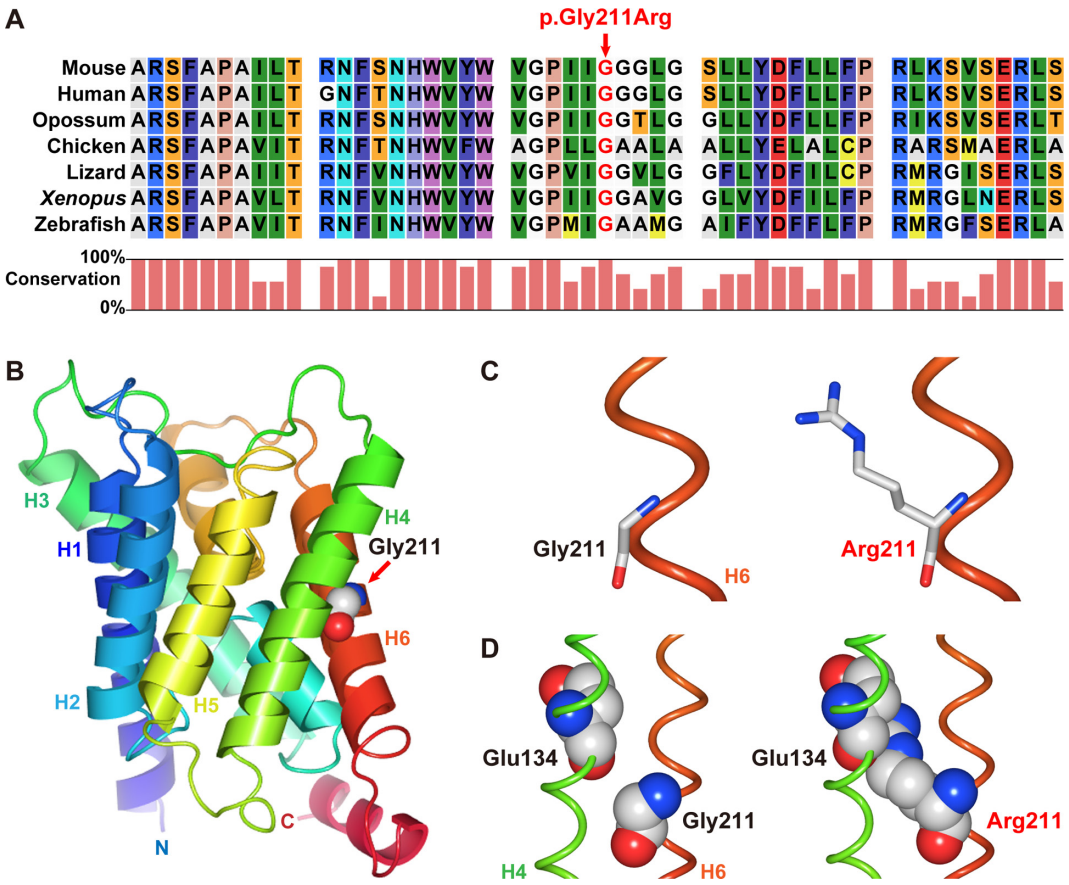

Fig. 4. Evolutionary and functional impact of the *Nat* mutation (p.Gly211Arg) in MIP. A. Evolutionary conservation of Gly211 in MIP. The top diagram shows an interspecies alignment. Arrow indicates the p.Gly211Arg mutation site. The bottom diagram indicates the conservation rates among the seven species. B. Ribbon diagram representations of MIP (PBD: 2B6O) [11]. The Gly211 residue in the *H6* domain is shown as a colored atom sphere. C. Stick representation of residue 211 of MIP on a B-spline diagram showing the substitution from glycine (neutral, left) to arginine (positive charged, right). D. Space-filling model of Gly211 (left) or Arg211 (right).

in the eyes of the Mip^{Nat} mutants. In wild-type and $Mip^{Nat/+}$ mice, approximately 26 kDa bands were detected (Fig. 5B). However, the signal was significantly decreased in $Mip^{Nat/+}$ mice (Figs. 5B and 5C). Moreover, no signals were obtained in the $Mip^{Nat/Nat}$ mice (Figs. 5B and 5C). Thus, we confirmed that the c.631A>G mutation results in a reduction of the *Mip* transcript in $Mip^{Nat/Nat}$ mice, and that the p.Gly211Arg mutation affects the expression levels of the MIP protein in $Mip^{Nat/+}$ and $Mip^{Nat/Nat}$ mice.

Effects of the Nat mutation on MIP expression and localization in the lens

The vertebrate lens is divided into two parts: the lens epithelium and lens fiber (Fig. 6A, left panel). The lens epithelial cells form a single cell layer on the anterior segment of the lens proliferate, which then migrate to the equator region, and then differentiate into fiber cells (Fig. 6A, middle panel) [4]. Moreover, organelles such as the cell nucleus and mitochondria are digested, the cell body is elongated, and the organelle-free zone forms in the nucleus of the lens during the differentiation of the lens fiber cells (Fig. 6A, right panel) [4]. In normal lens fiber cells, MIPs are widely expressed in the plasma membrane of the lens fiber cells (Fig. 6A). To estimate the effects of the p.Gly211Arg mutation on the MIP protein, we investigated its expression profile in the lens via immunohistochemistry.

MIP localized to the immature lens fiber cell membrane throughout the equator and the organelle-free zone in mice at P0 (Figs. 6B and 6C). Furthermore, MIP co-localized with CTNNB1, which has been reported to be

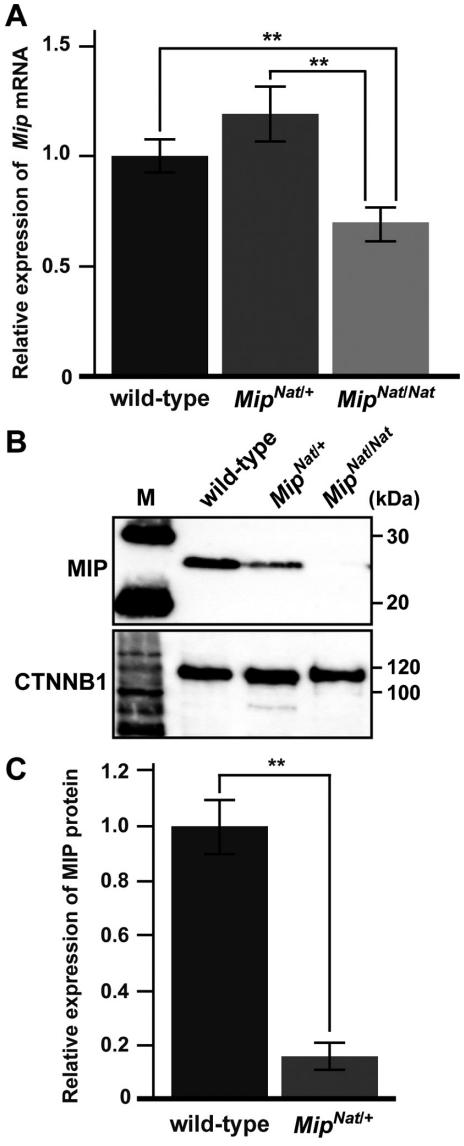

Fig. 5. Quantitative analyses of *Mip* transcript and MIP protein. A. Relative levels of *Mip* mRNA in the eye of wild-type, $Mip^{Nat/+}$, and $Mip^{Nat/Nat}$ mice at P0. B. Western blot analysis of MIP protein derived from the eye of wild-type, $Mip^{Nat/+}$, and $Mip^{Nat/Nat}$ mice at P1. Note the stepwise reduction of a single band at approximately 26-kDa as recognized by an anti-MIP antibody. The samples were processed for indirect immunofluorescence using an anti-CTNNB1 antibody. M: size standard (protein ladder). C. Relative levels of MIP proteins as detected by western blot analysis. $^{**}P<0.01$.

expressed in the lens fiber cell membrane, and also showed consistent localization with MIP [38]. However, we observed a different localization pattern for MIP in the lens of $Mip^{Nat/Nat}$ homozygous mice from that of the wild-type mice. The MIP fluorescent signals were detected in the perinuclear region of the immature lens fiber cells of $Mip^{Nat/Nat}$ mice (Fig. 6D). Interestingly, even though CTNNB1 localized normally, no signals for MIP were observed in the organelle-free zone of the $Mip^{Nat/Nat}$ mice (Fig. 6E). The normal expression patterns of MIP were observed in the lens of $Mip^{Nat/+}$ heterozygous mice. MIP was abundantly expressed without localization of the mutant MIP protein in the lens fiber cell membranes in both the equator region and the organelle-free zone of the immature lens (Figs. 6F and 6G). In the mature lens of P30 mice, we did not detect any changes in expression and localization at P0 in wild-type (Figs. 6H and 6I), $Mip^{Nat/Nat}$ (Figs. 6J and 6K), and $Mip^{Nat/+}$ (Figs. 6L and 6M) mice. Thus, our data clearly showed that the p.Gly211Arg mutation results in the mislocalization of MIP to the equator region and a loss of MIP in the organelle-free zone in $Mip^{Nat/Nat}$ mice. However, we did not observe any differences in MIP expression between the wild-type and $Mip^{Nat/+}$ mice.

Discussion

In this study, we identified a new missense mutation in *Mip* resulting in congenital semi-dominant cataracts. $Mip^{Nat/Nat}$ mice exhibited severe lens opacity, whereas only a mild phenotype was observed in $Mip^{Nat/+}$ mice (Figs. 1 and 2). A p.Gly211Arg mutation was detected in the *H6* domain of the MIP protein in the Mip^{Nat} mice (Figs. 3B and 3D). The Gly211 residue is conserved among representative vertebrates (Fig. 4A) and was shown via several bioinformatics analyses to have a high probability to be deleterious if this residue was mutated (Figs. 4B–4D). Moreover, we predicted that the Arg211 residue causes a disruption in the protein structure by crashing into the Glu134 residue in the *H4* domain, which may inhibit tetramer formation and/or traffic to the plasma membrane (Figs. 4C and 4D). Therefore, we strongly suggest that the p.Gly211Arg mutation in MIP is a causative mutation for the development of cataracts in Mip^{Nat} mutants.

In the lens of the $Mip^{Nat/Nat}$ homozygous mice, we were unable to detect MIP via western blot analysis (Fig. 5B). In the Mip^{Hfi} mutant mice, which lack 55 amino acids in the MIP protein as a result of a 76-bp deletion, the mutant protein was less stable [29]. In humans, the $MIP^{p.219*}$ mutant allele also showed a reduction in mutant proteins levels in *in vitro* experiments [30]. Although mRNA transcripts could be detected for these mutant

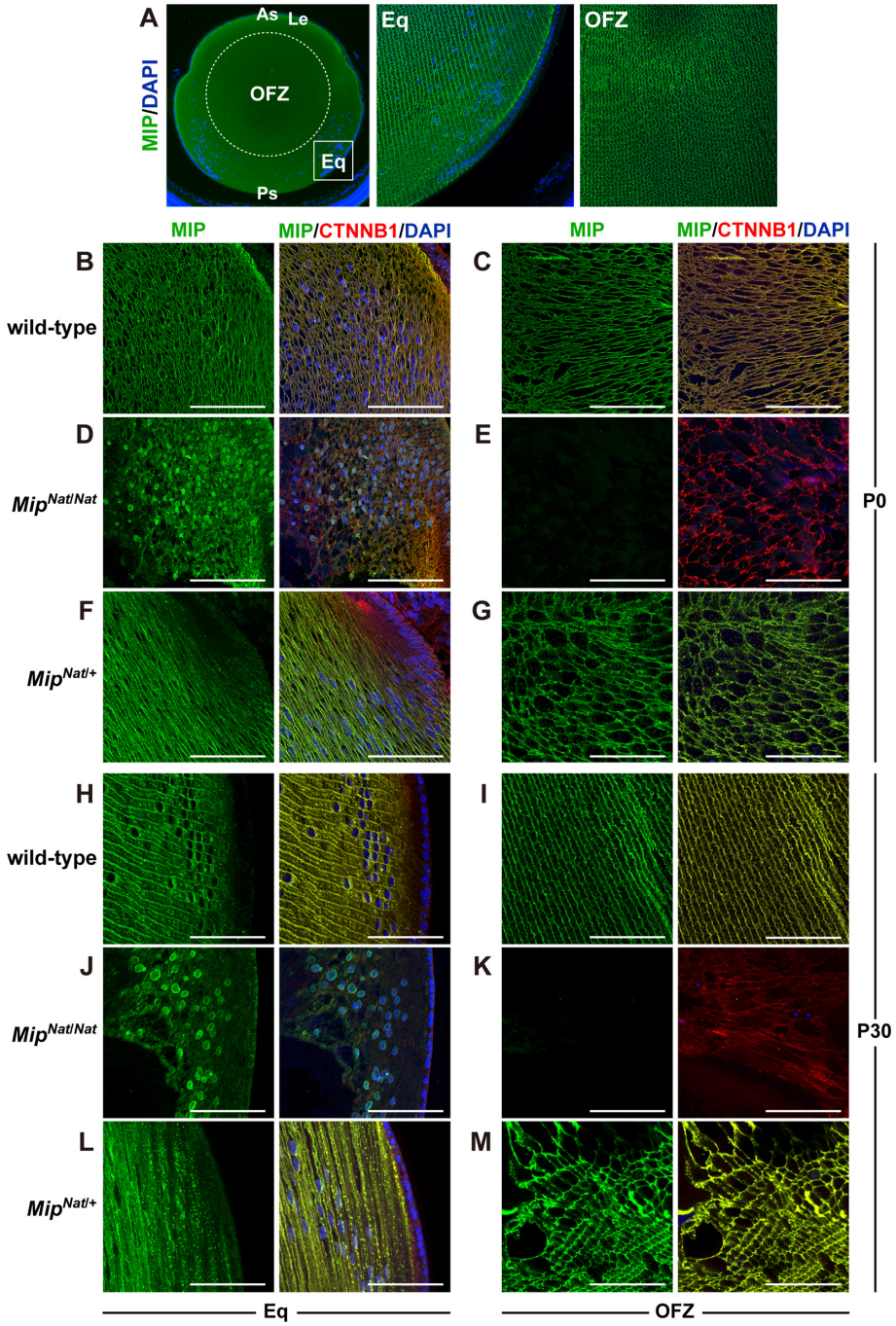

Fig. 6. Immunohistochemistry of MIP in the lens of *Nat* mutants. A. Immunofluorescent staining with anti-MIP antibody (green) and DAPI (blue) showing normal expression and localization in the whole lens (left), the equator region (Eq) (middle), and the organelle-free zone (OFZ) (right) of adult wild-type mice at P70. As, anterior segment; Ps, posterior segment; and Le, lens epithelium. B–M. Immunofluorescent staining for MIP (green), CTNNB1 (red), and DAPI (blue) in the lens of wild-type (B, C, H, and I), $Mip^{Nat/Nat}$ (D, E, J, and K), and $Mip^{Nat/+}$ (F, G, L, and M) mice at P0 (B–G) and P30 (H–M). Highly magnified images of the Eq (B, D, F, H, J, and L) and OFZ (C, E, G, I, K, and M) are shown. Scale bar=100 μm.

alleles, the translated products were drastically reduced. This feature probably indicates that these missense mutations result in the destabilization of the translated protein. The Mip^{Hfi} and $MIP^{p.219*}$ mutant alleles affect the transmembrane region of the *H4–H5* and *H6* domains, respectively (Fig. 3D) [29, 30], suggesting that

mutations in the transmembrane region results in the loss of MIP protein stability. Furthermore, since the Arg211 residue in Mip^{Nat} mice is located in the transmembrane domain, we predicted that the p.Gly211Arg mutation also decreases the stability of MIP (Figs. 5B and 5C). Moreover, we showed that a substitution at residue 211, an evolutionarily conserved amino acid, in the *H6* domain of MIP results in an abnormal expression pattern in the perinuclear region on the lens fiber cells (Figs. 6D and 6J). Previous studies have shown that MIP is mislocalized to the perinuclear region in the homozygous mutants of the $Mip^{Cat\text{-}Lop}$, $Mip^{Cat\text{-}Fr}$, Mip^{Hfi} *and* $Mip^{Cat\text{-}Tohm}$ alleles [23, 27, 29]. Studies *in vitro* also confirmed that several *MIP* mutations in humans result in an abnormal localization of MIP [7, 8, 26, 30]. In addition, Zhou *et al.* recently reported that the lens fiber degeneration in mutant MIP lens is caused by cell-death via the endoplasmic reticulum (ER) stress in $Mip^{Cat\text{-}Lop/+}$ mice [44]. Therefore, we hypothesized that the abnormal perinuclear expression of MIP results in it being digested in the ER, and which may then lead to the reduction of mutant MIP protein, such as that observed in $Mip^{Nat/Nat}$ mice.

Furthermore, we showed here that the $Mip^{Nat/+}$ mice also develop cataracts (Figs. 1C and 1D). In theory of formal genetics, the onsets of phenotypes in heterozygous animals can be explained by a gain-of-function effect, dominant negative effect, or haploinsufficiency [31]. The dominant effects of *MIP*/*Mip* mutations of humans and mice are also suggested the cataractgenesis based on the genetic theories. For example, several studies are indicated that abnormal mislocalization of MIP to the perinuclear region results in the development of dominant cataracts via interference of the wild-type protein by the mutant protein [8, 30, 44]. These findings suggest that mutant MIP can be cytotoxic, implying that these mutants develop cataracts through a gain-of-function effect. However, there were no differences between the expression pattern of MIP in the lens of the wild-type and $Mip^{Nat/+}$ mice (Fig. 6). Therefore, we predict that it is unlikely for $Mip^{Nat/+}$ mice to develop cataracts by a mutant MIP gain-of-function effect of the mutant MIP protein. In contrast, other previous reports have suggested that mutant MIP may also have dominant-negative effects. Francis *et al.* performed injections of cRNAs encoding human 134G and 138R mutant MIP proteins into *X. laevis* oocytes, resulting in a reduction in water permeability and the localization of both mutant proteins to the cytoplasmic space [8]. This was shown in an experiment where both wild-type and mutant MIP proteins were co-expressed in *X. laevis* oocytes [8]. Furthermore, Song *et al.* also reported the development of cataracts by a dominant-negative effect as a result of a $MIP^{p.Tyr219*}$ mutation in MIP, which was observed in a Chinese family [30]. The mutant protein derived from the $MIP^{p.Tyr219*}$ co-localizes with wild-type MIP in the cytoplasm, suggesting that the mutant MIP functions to inhibit trafficking of wild-type MIP to the plasma membrane [30]. This may also be the case in the development of cataracts in $Mip^{Nat/+}$ mice because MIP localization in the lens of $Mip^{Nat/+}$ mice is similar to that of the wild-type mice (Fig. 6). Furthermore, MIP haploinsufficiency is likely to be a more acceptable genetic mechanism to describe the development of cataracts in $Mip^{Nat/+}$ mice because we observed massive reduction of MIP in eye-derived protein by western blot analysis in Mip^{Nat} mutants (Figs. 5B and 5C). The cataract phenotypes are milder than those of the $Mip^{Nat/Nat}$ mice (Figs. 1 and 2), which appear to be similar to $Mip^{+/-}$ mice [28].

Although we could not completely explain the molecular mechanism underlying the massive reduction of MIP in Mip^{Nat} mutants, we may have been unable to detect the mutant MIP via western blotting due to an aggregation of the mutant MIP into the ER without it being trafficked to the plasma membrane, or its rapid degradation in ER. The massive reduction of mutant MIP due to the complete loss of expression was also observed in the organelle-free zone of $Mip^{Nat/Nat}$ mice lens (Figs. 6E and 6K) because aggregated proteins in the ER can be extracted from the insoluble fraction of the eye. Generally, the mutant proteins such as those that misfolded, are degraded by cellular proteases via protein quality control system [39]. Many diverse mutant proteins are unable to progress beyond the ER to their correct sites of action, such as the plasma membrane or the outside the cell following secretion [39]. For aquaporin-2, one of the members of the aquaporin family, several mutant versions of this protein mislocalized to the ER where it was degraded [32]. However, the speculations mentioned above have a fatal logical flaw because it is inconsistent with the observations of reduced MIP in $Mip^{Nat/+}$ mice. The MIP protein levels in the eyes of $Mip^{Nat/+}$ mice were less than half of that of wild-type mice as shown via western blot analysis (Figs. 5B and 5C). However, there were no differences in MIP expression levels between the wild-type and $Mip^{Nat/+}$ mice as shown via immuno-

histochemistry of lens (Fig. 6). In addition, we cannot explain the significant reduction of *Mip* transcript in $Mip^{Nat/Nat}$ mice (Fig. 5A). We suggest that the reduction of *Mip* transcript in $Mip^{Nat/Nat}$ mice was not dependent on the missense mutation because no significant differences of *Mip* expression between wild-type and $Mip^{Nat/+}$ mice were observed. Thus, our results provided a new interesting phenomenon concerning changes in gene and protein expression; however, we cannot fully explain the molecular mechanism as yet, as demonstrated in this study.

Cataracts are a profound and common eye disease in human populations [2, 9, 24], and many gene mutations related to the development of cataracts have been identified [5, 12, 14, 15]. The mutations in *MIP* are some of the most frequently observed causes of cataracts in human. The Mip^{Nat} allele is the 2nd case of semi-dominant cataracts caused by a missense mutation, and is the first report of a missense mutation affecting the *H6* domain of MIP. Therefore, we suggest that the Mip^{Nat} mice may be a useful model for studying the role of MIP in maintaining lens transparency, as well as the detailed pathology of human cataracts as a result of missense mutations in the *H6*-encoding region of *MIP*.

Acknowledgments

This work was financially supported by the Sasakawa Scientific Research Grant (Grant Number 26–518 to G.T) from the Japan Science Society; and the grant from Graduate School of Bioindustry, Tokyo University of Agriculture. We also thank Moeko Takahashi for technical assistance.

References

1. Adzhubei, I.A., Schmidt, S., Peshkin, L., Ramensky, V.E., Gerasimova, A., Bork, P., Kondrashov, A.S., and Sunyaev, S.R. 2010. A method and server for predicting damaging missense mutations. *Nat. Methods* 7: 248–249. [Medline] [CrossRef]
2. Asbell, P.A., Dualan, I., Mindel, J., Brocks, D., Ahmad, M., and Epstein, S. 2005. Age-related cataract. *Lancet* 365: 599–609. [Medline] [CrossRef]
3. Berry, V., Francis, P., Kaushal, S., Moore, A., and Bhattacharya, S. 2000. Missense mutations in MIP underlie autosomal dominant 'polymorphic' and lamellar cataracts linked to 12q. *Nat. Genet.* 25: 15–17. [Medline] [CrossRef]
4. Chepelinsky, A.B. 2009. Structural function of MIP/aquaporin 0 in the eye lens; genetic defects lead to congenital inherited cataracts. *Handb. Exp. Pharmacol.* 190: 265–297. [Medline] [CrossRef]
5. Churchill, A. and Graw, J. 2011. Clinical and experimental advances in congenital and paediatric cataracts. *Philos. Trans. R. Soc. Lond. B Biol. Sci.* 366: 1234–1249. [Medline] [CrossRef]
6. Choi, Y., Sims, G.E., Murphy, S., Miller, J.R., and Chan, A.P. 2012. Predicting the functional effect of amino acid substitutions and indels. *PLoS One* 7: e46688. [Medline] [CrossRef]
7. Ding, X., Zhou, N., Lin, H., Chen, J., Zhao, C., Zhou, G., Hejtmancik, J.F., and Qi, Y. 2014. A novel MIP gene mutation analysis in a Chinese family affected with congenital progressive punctate cataract. *PLoS One* 9: e102733. [Medline] [CrossRef]
8. Francis, P., Chung, J.J., Yasui, M., Berry, V., Moore, A., Wyatt, M.K., Wistow, G., Bhattacharya, S.S., and Agre, P. 2000. Functional impairment of lens aquaporin in two families with dominantly inherited cataracts. *Hum. Mol. Genet.* 9: 2329–2334. [Medline] [CrossRef]
9. Foster, A. and Resnikoff, S. 2005. The impact of Vision 2020 on global blindness. *Eye (Lond.)* 19: 1133–1135. [Medline] [CrossRef]
10. Geyer, D.D., Spence, M.A., Johannes, M., Flodman, P., Clancy, K.P., Berry, R., Sparkes, R.S., Jonsen, M.D., Isenberg, S.J., and Bateman, J.B. 2006. Novel single-base deletional mutation in major intrinsic protein (MIP) in autosomal dominant cataract. *Am. J. Ophthalmol.* 141: 761–763. [Medline] [CrossRef]
11. Gonen, T., Cheng, Y., Sliz, P., Hiroaki, Y., Fujiyoshi, Y., Harrison, S.C., and Walz, T. 2005. Lipid-protein interactions in double-layered two-dimensional AQP0 crystals. *Nature* 438: 633–638. [Medline] [CrossRef]
12. Graw, J. 2009. Mouse models of cataract. *J. Genet.* 88: 469–486. [Medline] [CrossRef]
13. Gu, F., Zhai, H., Li, D., Zhao, L., Li, C., Huang, S., and Ma, X. 2007. A novel mutation in major intrinsic protein of the lens gene (MIP) underlies autosomal dominant cataract in a Chinese family. *Mol. Vis.* 13: 1651–1656. [Medline]
14. Hejtmancik, J.F. 2008. Congenital cataracts and their molecular genetics. *Semin. Cell Dev. Biol.* 19: 134–149. [Medline] [CrossRef]
15. Huang, B. and He, W. 2010. Molecular characteristics of inherited congenital cataracts. *Eur. J. Med. Genet.* 53: 347–357. [Medline] [CrossRef]
16. Ionides, A., Francis, P., Berry, V., Mackay, D., Bhattacharya, S., Shiels, A., and Moore, A. 1999. Clinical and genetic heterogeneity in autosomal dominant cataract. *Br. J. Ophthalmol.* 83: 802–808. [Medline] [CrossRef]
17. Kumari, S.S., Gandhi, J., Mustehsan, M.H., Eren, S., and Varadaraj, K. 2013. Functional characterization of an AQP0 missense mutation, R33C, that causes dominant congenital lens cataract, reveals impaired cell-to-cell adhesion. *Exp. Eye Res.* 116: 371–385. [Medline] [CrossRef]
18. Larkin, M.A., Blackshields, G., Brown, N.P., Chenna, R., McGettigan, P.A., McWilliam, H., Valentin, F., Wallace, I.M., Wilm, A., Lopez, R., Thompson, J.D., Gibson, T.J., and Higgins, D.G. 2007. Clustal W and Clustal X version 2.0. *Bioinformatics* 23: 2947–2948. [Medline] [CrossRef]

19. Lin, H., Hejtmancik, J.F., and Qi, Y. 2007. A substitution of arginine to lysine at the COOH-terminus of MIP caused a different binocular phenotype in a congenital cataract family. *Mol. Vis.* 13: 1822–1827. [Medline]
20. Ma, A.S., Grigg, J.R., Ho, G., Prokudin, I., Farnsworth, E., Holman, K., Cheng, A., Billson, F.A., Martin, F., Fraser, C., Mowat, D., Smith, J., Christodoulou, J., Flaherty, M., Bennetts, B., and Jamieson, R.V. 2016. Sporadic and Familial Congenital Cataracts: Mutational Spectrum and New Diagnoses Using Next-Generation Sequencing. *Hum. Mutat.* 37: 371–384. [Medline] [CrossRef]
21. Mulders, S.M., Preston, G.M., Deen, P.M., Guggino, W.B., van Os, C.H., and Agre, P. 1995. Water channel properties of major intrinsic protein of lens. *J. Biol. Chem.* 270: 9010–9016. [Medline] [CrossRef]
22. Ng, P.C. and Henikoff, S. 2001. Predicting deleterious amino acid substitutions. *Genome Res.* 11: 863–874. [Medline] [CrossRef]
23. Okamura, T., Miyoshi, I., Takahashi, K., Mototani, Y., Ishigaki, S., Kon, Y., and Kasai, N. 2003. Bilateral congenital cataracts result from a gain-of-function mutation in the gene for aquaporin-0 in mice. *Genomics* 81: 361–368. [Medline] [CrossRef]
24. Sacca, S.C., Bolognesi, C., Battistella, A., Bagnis, A., and Izzotti, A. 2009. Gene-environment interactions in ocular diseases. *Mutat. Res.* 667: 98–117. [Medline] [CrossRef]
25. Senthil Kumar, G., Kyle, J.W., Minogue, P.J., Dinesh Kumar, K., Vasantha, K., Berthoud, V.M., Beyer, E.C., and Santhiya, S.T. 2013. An MIP/AQP0 mutation with impaired trafficking and function underlies an autosomal dominant congenital lamellar cataract. *Exp. Eye Res.* 110: 136–141. [Medline] [CrossRef]
26. Shentu, X., Miao, Q., Tang, X., Yin, H., and Zhao, Y. 2015. Identification and Functional Analysis of a Novel MIP Gene Mutation Associated with Congenital Cataract in a Chinese Family. *PLoS One* 10: e0126679. [Medline] [CrossRef]
27. Shiels, A. and Bassnett, S. 1996. Mutations in the founder of the MIP gene family underlie cataract development in the mouse. *Nat. Genet.* 12: 212–215. [Medline] [CrossRef]
28. Shiels, A., Bassnett, S., Varadaraj, K., Mathias, R., Al-Ghoul, K., Kuszak, J., Donoviel, D., Lilleberg, S., Friedrich, G., and Zambrowicz, B. 2001. Optical dysfunction of the crystalline lens in aquaporin-0-deficient mice. *Physiol. Genomics* 7: 179–186. [Medline] [CrossRef]
29. Sidjanin, D.J., Parker-Wilson, D.M., Neuhäuser-Klaus, A., Pretsch, W., Favor, J., Deen, P.M., Ohtaka-Maruyama, C., Lu, Y., Bragin, A., Skach, W.R., Chepelinsky, A.B., Grimes, P.A., and Stambolian, D.E. 2001. A 76-bp deletion in the *Mip* gene causes autosomal dominant cataract in *Hfi* mice. *Genomics* 74: 313–319. [Medline] [CrossRef]
30. Song, Z., Wang, L., Liu, Y., and Xiao, W. 2015. A novel nonsense mutation in the MIP gene linked to congenital posterior polar cataracts in a Chinese family. *PLoS One* 10: e0119296. [Medline] [CrossRef]
31. Strachan, T. and Read, A. 2010. Human Molecular Genetics, 4th ed., Garland Science, New York.
32. Tamarappoo, B.K. and Verkman, A.S. 1998. Defective aquaporin-2 trafficking in nephrogenic diabetes insipidus and correction by chemical chaperones. *J. Clin. Invest.* 101: 2257–2267. [Medline] [CrossRef]
33. Verkman, A.S. 2009. Knock-out models reveal new aquaporin functions. *Handb. Exp. Pharmacol.* 190: 359–381. [Medline] [CrossRef]
34. Wada, K., Maeda, Y.Y., Watanabe, K., Oshio, T., Ueda, T., Takahashi, G., Yokohama, M., Saito, J., Seki, Y., Takahama, S., Ishii, R., Shitara, H., Taya, C., Yonekawa, H., and Kikkawa, Y. 2011. A deletion in a *cis* element of *Foxe3* causes cataracts and microphthalmia in *rct* mice. *Mamm. Genome* 22: 693–702. [Medline] [CrossRef]
35. Wada, K., Matsushima, Y., Tada, T., Hasegawa, S., Obara, Y., Yoshizawa, Y., Takahashi, G., Hiai, H., Shimanuki, M., Suzuki, S., Saitou, J., Yamamoto, N., Ichikawa, M., Watanabe, K., and Kikkawa, Y. 2014. Expression of truncated PITX3 in the developing lens leads to microphthalmia and aphakia in mice. *PLoS One* 9: e111432. [Medline] [CrossRef]
36. Wang, W., Jiang, J., Zhu, Y., Li, J., Jin, C., Shentu, X., and Yao, K. 2010. A novel mutation in the major intrinsic protein (MIP) associated with autosomal dominant congenital cataracts in a Chinese family. *Mol. Vis.* 16: 534–539. [Medline]
37. Wang, K.J., Li, S.S., Yun, B., Ma, W.X., Jiang, T.G., and Zhu, S.Q. 2011. A novel mutation in MIP associated with congenital nuclear cataract in a Chinese family. *Mol. Vis.* 17: 70–77. [Medline]
38. Watanabe, K., Wada, K., Ohashi, T., Okubo, S., Takekuma, K., Hashizume, R., Hayashi, J., Serikawa, T., Kuramoto, T., and Kikkawa, Y. 2012. A 5-bp insertion in *Mip* causes recessive congenital cataract in KFRS4/Kyo rats. *PLoS One* 7: e50737. [Medline] [CrossRef]
39. Waters, P.J. 2001. Degradation of mutant proteins, underlying "loss of function" phenotypes, plays a major role in genetic disease. *Curr. Issues Mol. Biol.* 3: 57–65. [Medline]
40. Xiao, X., Li, W., Wang, P., Li, L., Li, S., Jia, X., Sun, W., Guo, X., and Zhang, Q. 2011. Cerulean cataract mapped to 12q13 and associated with a novel initiation codon mutation in *MIP*. *Mol. Vis.* 17: 2049–2055. [Medline]
41. Yang, G., Zhang, G., Wu, Q., and Zhao, J. 2011. A novel mutation in the *MIP* gene is associated with autosomal dominant congenital nuclear cataract in a Chinese family. *Mol. Vis.* 17: 1320–1323. [Medline]
42. Yu, Y., Yu, Y., Chen, P., Li, J., Zhu, Y., Zhai, Y., and Yao, K. 2014. A novel *MIP* gene mutation associated with autosomal dominant congenital cataracts in a Chinese family. *BMC Med. Genet.* 15: 6. [Medline] [CrossRef]
43. Zeng, L., Liu, W., Feng, W., Wang, X., Dang, H., Gao, L., Yao, J., and Zhang, X. 2013. A novel donor splice-site mutation of major intrinsic protein gene associated with congenital cataract in a Chinese family. *Mol. Vis.* 19: 2244–2249. [Medline]
44. Zhou, Y., Bennett, T.M., and Shiels, A. 2016. Lens ER-stress response during cataract development in *Mip*-mutant mice. *Biochim. Biophys. Acta* 1862: 1433–1442. [Medline] [CrossRef]